

5

Pairing vibrations

When the strength G of the pairing interaction is greater than a critical value G_c , the gap equation has a non-zero solution for the gap parameter Δ and the BCS ground state of a system of nucleons is stable. Single nucleon levels are partially occupied in an energy range Δ around the Fermi energy λ . The BCS state is not an eigenstate of nucleon number and violates gauge invariance. Pairing vibrations, which are fluctuations about the BCS state, were studied in Chapter 4 and it was shown that gauge invariance was restored within the framework of the random phase approximation (RPA). In this chapter we study the question of pairing vibrations within a more general context, considering also pairing vibrations in normal nuclei which have pairing strengths $G < G_c$ and $\Delta = 0$. To a first approximation single-particle levels are occupied with unit probability up to the Fermi energy and with zero probability for states above the Fermi level. Pairing vibrations modify this simple picture and are associated with fields which change the number of particles by 2. They produce correlations which enhance or modify pair transfer amplitudes. Parts of this chapter is based on Broglia and Riedel (1967a,b) and Broglia *et al.* (1973) (see also Anderson (1958), Högaasen-Feldman (1961), Bes and Broglia (1966), Bohr and Mottelson (1975), Ring and Schuck (1980), Wölfle (1972, 1978), Schmidt (1972)).

5.1 The two-level model

The simplest model which displays fluctuations of the pairing gap contains two j -shells which may have the same or different degeneracy, and which are separated by a distance D . Pairs of particles are scattered in these orbitals by a pairing force with constant matrix elements. A solution of the two-level model was given by Högaasen-Feldman (1961). More generally the exact eigenstates for a pairing force with constant matrix elements distributed in an arbitrary number of levels was found by Richardson and Sherman (1964) (see Section 2.8).

The two-level model Hamiltonian can be written as

$$H = \frac{D}{2}(N_{j_2} - N_{j_1}) - \frac{1}{4}G(P_{j_1}^\dagger + P_{j_2}^\dagger)(P_{j_1} + P_{j_2}), \quad (5.1)$$

where

$$P_{j_1}^\dagger = \sum_{m>0} (-1)^{j+m} a_{jm}^\dagger a_{j-m}^\dagger = -\sqrt{\Omega} [a_j^\dagger a_j^\dagger]_0^0, \\ N_j = \sum_m a_{jm}^\dagger a_{jm}, \quad \Omega = \frac{2j+1}{2}, \quad (j = j_1, j_2). \quad (5.2)$$

The two-level model does not have an analytical solution, although it allows for a rather simple numerical solution in the orthonormal basis

$$|m, n-m\rangle = M_m^{-1} (P_{j_1}^\dagger)^m (P_{j_2}^\dagger)^{n-m} |0\rangle, \quad (5.3)$$

n being the total number of pairs of particles in the system. The matrix element of the Hamiltonian (5.1) in this basis is

$$\langle m', n-m' | H | m, n-m \rangle = \delta(m, m') \\ \times [(n-2m)D - G(m(\Omega_1 + 1 - m) + (n-m)(\Omega_2 + 1 - n + m))]^{1/2} \\ - \delta(m', (m-1))G[m(\Omega_1 + 1 - m)(n-m+1)(\Omega_2 - n + m)]^{1/2} \\ - \delta(m', (m+1))G[(m+1)(\Omega_1 - m)(n-m)(\Omega_2 + 1 - n + m)]^{1/2}. \quad (5.4)$$

To obtain the solution of the model one has thus to diagonalize a codiagonal matrix.

As discussed in Chapters 2 and 3, two-particle transfer processes are the specific tools to study the pairing degrees of freedom, in particular pairing vibrations. The model operator which induces such processes is defined as

$$T = P_1^\dagger + P_2^\dagger. \quad (5.5)$$

In the basis (5.3) the T operator has the following matrix elements

$$\langle m', n+1-m' | T | m, n-m \rangle \\ = \delta(m', m)[(n-m+1)(\Omega_2 - n + m)]^{1/2} \\ + \delta(m', (m+1))[(m+1)(\Omega_1 - m)]^{1/2}. \quad (5.6)$$

The two-particle transfer cross-section can be shown to be proportional to the square of the matrix element (5.6) (see e.g. Broglia *et al.* (1973)).

From the commutation relation $[N_i, P_j^\dagger] = 2\delta(i, j)P_j^\dagger$ one can calculate the occupation number of the two orbits

$$\langle \alpha | N_1 | \alpha \rangle = 2 \sum_m m |c_{n,m}|^2, \\ \langle \alpha | N_2 | \alpha \rangle = 2 \sum_m (n-m) |c_{n,m}|^2, \quad (5.7)$$

where the eigenfunction of the total Hamiltonian is

$$|\alpha\rangle = \sum_m c_{n,m} |m, n - m\rangle. \quad (5.8)$$

For $\Omega_1 = \Omega_2 = \Omega$ there are two dimensionless parameters in the model. The first is chosen to be Ω (see equation (5.2)) and it gives a measure of the phase space which the particles have at their disposal to correlate. The second is

$$x = 2G \frac{\Omega}{D} \quad (5.9)$$

and measures the interplay between the pairing strength and the shell effects.

In Fig. 5.1 we display the energies, cross-sections and occupation amplitudes associated with a system $\Omega_1 = \Omega_2 = \Omega = 20$ and $x = 0.5$ and $x = 2.0$ as a function of the number of pairs n ($18 \leq n \leq 22$). When $n = \Omega$, the lower level is full and the upper level is empty in the limit $x \rightarrow 0$. In the case $x = 0.5$ the coupling is weak and there is only one characteristic energy, the spacing D between the two single-particle levels.

Any level lies at approximately an integer number of times this energy with respect to the ground state, forming a (harmonic) pairing vibrational band. The two-nucleon transfer cross-section associated with transitions between ground states is proportional to $|n - \Omega|$, i.e. to the absolute value of the number of pairs missing from or in excess of the closed shell. All the first-excited-state stripping cross-sections for $n - \Omega < 0$ are equal and their common value is close to $|\langle \text{gs}(n = 20) | T | \text{gs}(n = 19) \rangle|^2$. On the other hand, none of the lowest excited states with $n - \Omega \geq 0$ is populated in such reactions. This is also true for the second and higher excited states for $n - \Omega \leq 0$. A similar pattern is observed for two-nucleon pickup processes.

For the case of $x = 2$ the energy of the states follows a parabolic distribution (pairing rotational band, see Chapter 4) as a function of the number of particles. There are two characteristic energies, corresponding to interband and intraband spacing. The situation is very similar to the one encountered in the case of a single j -shell (see equation (4.57), also Appendix H). In this case, however, there is a finite cross-section to the excited states, although an order of magnitude smaller than between states lying in the same energy parabola. The situation for $x = 1.2$ is intermediate to the one observed for $x = 0.5$ and $x = 2$.

The probability amplitude $|c_{n,m}|^2$ associated with the ground state of the closed-shell system ($n - \Omega = 0$) is also given in Fig. 5.1 as a function of $n - m$. Note that a major change takes place in going from $x = 0.5$ to $x = 2.0$, indicating a change in the coupling scheme of the nucleons correlated through the pairing interaction. Similar results to those displayed in Fig. 5.1 are obtained for $\Omega_1 \neq \Omega_2$ (see Broglia and Sørensen (1968)). One can, however, distinguish in this case two typical energies and two basic two-particle transfer cross-sections,

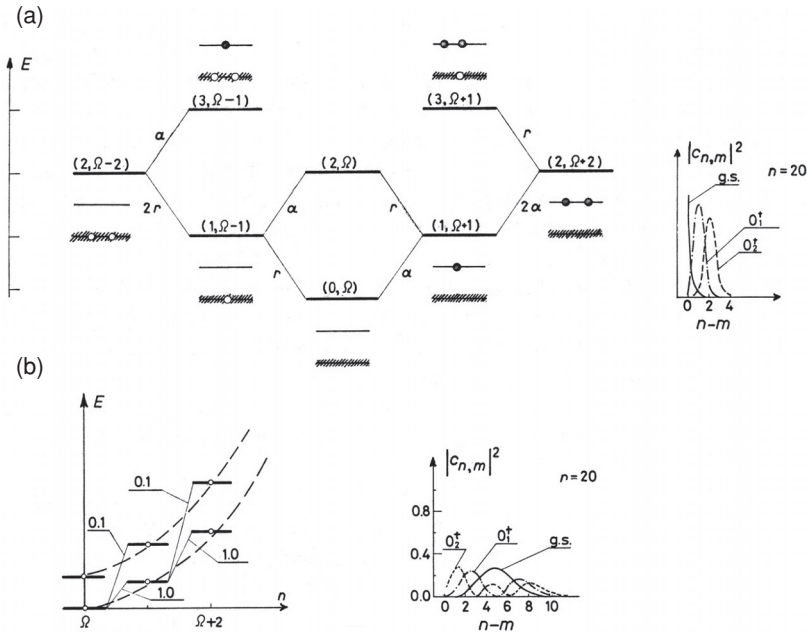


Figure 5.1. Schematic representation of the solution of the two-level model for $\Omega_1 = \Omega_2 = 20$ and for different values of x and n . In (a) the results for $x = 0.5$ are displayed. Because of the particular degeneracy of the model, the energy of the ground state of the system with $n = \Omega \pm 1$ pairs of particles is the same when measured with respect to the closed-shell system (see, however, Sections 5.2 and 8.4). All two-particle transition probabilities are measured in terms of $a = \sigma(\text{gs}(\Omega_1) \rightarrow \text{gs}(\Omega_1 + 1))$ and of $r = \sigma(\text{gs}(\Omega_1) \rightarrow \text{gs}(\Omega_1 - 1))$. Because of the particular symmetry of the model $a = r$. For each level of the spectrum, which is identified by the quantum numbers (N, n) , a schematic representation of the main component of the wavefunction is shown. The corresponding square amplitudes $|c_{n,m}|^2$ (see equations (5.7) and (5.8)) associated with the ground state and low excited states of the $n = \Omega_1$ system are also shown. In (b) the energies and two-particle cross-sections for $x = 2.0$ associated with the ground and the first excited states of the systems with $n \geq \Omega_1$ are displayed. The quantities $|c_{n,m}|^2$ corresponding to the ground state and two lowest excited states are also displayed.

one associated with the removal of a pair and the other with the addition of a pair (see Figs. 5.5 and 8.17).

5.1.1 Collective treatment of pairing vibrations; normal systems ($x < 1$)

The different levels of the pairing spectrum obtained by diagonalizing the Hamiltonian defined in equation (5.1) for $x < 1$ and reported in Fig. 5.1 can be labelled by the number of pairs n and by a number N indicating their energy sequence in the spectrum. The lowest state corresponds to a closed-shell system and has $(N = 0, n = \Omega)$. The two lowest excited states have the same energy E and are labelled $(N = 1, n = \Omega + 1)$ and $(N = 1, n = \Omega - 1)$ respectively. The next

excitation energy is $2E$ and corresponds to a triplet of states comprising the two states ($N = 2, n = \Omega \pm 2$) and ($N = 2, n = \Omega$). This spectrum is characteristic of a two-dimensional harmonic oscillator, where N indicates the number of phonons, while $\hbar n$ plays the role of the angular momentum in two dimensions. The values of the transfer cross-sections as well as the associated selection rules further confirm the harmonic structure of the spectrum. One of the degrees of freedom of the two-dimensional oscillator is associated with the change in the number of pairs in the shell above the Fermi surface (pair addition mode) and the other with the change in the number of pairs in the shell below the Fermi surface (pair removal mode).

It is thus natural to rewrite the Hamiltonian (5.1) as

$$H = (W_a \Gamma_a^\dagger \Gamma_a + W_r \Gamma_r^\dagger \Gamma_r), \quad (5.10)$$

where Γ_a^\dagger and Γ_r^\dagger are the creation operators of the pair addition and pair removal modes, which are expressed in terms of the operators P_j^\dagger and P_j as

$$\begin{aligned} \Gamma_a^\dagger &= a_2 P_2^\dagger + a_1 P_1^\dagger, \\ \Gamma_r^\dagger &= r_1 P_1 + r_2 P_2. \end{aligned} \quad (5.11)$$

Note that the definition introduced in equation (5.10) is equivalent (in the quasi-beam approximation) to the relations $[H, \Gamma_a^\dagger] = W_a \Gamma_a^\dagger$ and $[H, \Gamma_r^\dagger] = W_r \Gamma_r^\dagger$ (see Appendix A, equation (A.68)).

Assuming the relation

$$[P_j, P_{j'}^\dagger] = (\Omega - N_j) \delta(j, j') \approx \Omega \delta(j, j') \quad (5.12)$$

to be valid for any state of the system under discussion, one obtains

$$a_2 = r_1 = -\frac{2G\sqrt{\Omega}}{(1-x)^{1/4}(2D-W)} \quad (5.13)$$

and

$$a_1 = r_2 = \frac{2G\sqrt{\Omega}}{(1-x)^{1/4}(2D+W)}, \quad (5.14)$$

where

$$W = W_a = W_r = 2D(1-x)^{1/2} \quad (5.15)$$

is the common energy of the pairing modes of excitation. The intensity with which the pair addition and pair removal modes are excited is

$$\begin{aligned} |\langle n_a = 1, n_r | T | n_a = 0, n_r \rangle|^2 &= (a_2 - a_1)^2 \Omega^2 \\ &= |\langle n_a, n_r = 1 | T | n_a, n_r = 0 \rangle|^2 = (r_2 - r_1)^2 \Omega^2 \\ &= \Omega(1-x)^{-1/2}. \end{aligned} \quad (5.16)$$

The above results reproduce the main features of the exact calculations for $x < 1$. Acting with Γ_a^\dagger and Γ_r^\dagger on the vacuum state, one can build the whole pairing spectrum. A general state is given by

$$|n_a, n_r\rangle = \frac{1}{\sqrt{n_a!n_r!}}(\Gamma_a^\dagger)^{n_a}(\Gamma_r^\dagger)^{n_r}|n_a = 0, n_r = 0\rangle. \quad (5.17)$$

The RPA solution is valid for small values of x . As x increases, W decreases and the cross-sections associated with the two modes tend to ∞ . The transition between the normal and the superfluid phase takes place for $x = 1$. Similar features to the one discussed above are also observed in the phase transition between spherical and quadrupole deformed nuclei. In this case the electromagnetic-transition probability plays the role of the two-nucleon transfer cross-section. The analogy between surface and pairing modes can be carried quite far as discussed in Broglia *et al.* (1973) (see also Belyaev (1972) and Schmidt (1972)). The theory of pairing vibrations can also be cast in terms of the collective variables α, ϕ as done in the case of pairing rotations. In fact, in these variables it is possible to formulate the problem of the pairing modes through a Hamiltonian which treats rotations and vibrations on an equal footing (see Bes *et al.* (1970)). For $\Delta \sim 0$, the energies associated with fluctuations in α and ϕ are comparable.

5.1.2 Collective treatment of pairing vibrations; superfluid systems ($x > 1$)

The main static effects of the pairing correlations for $x > 1$ can be taken into account through the quasiparticle transformation, which implies a complete hybridization of particles and holes, and thus an intrinsic system connected with the laboratory system through a rotation in gauge space (see Chapter 4 and Appendix I). As discussed in Chapter 3 and in Appendix G, the pairing Hamiltonian approximately reduces to the independent quasiparticle Hamiltonian

$$H_{11} = \sum_j E_j [\alpha_j^\dagger \alpha_j]_0^0, \quad (5.18)$$

where E_j are quasiparticle energies and $\alpha_{jm}^\dagger, \alpha_{jm}$ are quasiparticle creation and annihilation operators respectively. The symbol $[\]_0^0$ implies that these operators are coupled to angular momentum zero, and consequently also zero magnetic quantum number. In the present section we review the different types of collective modes generated by the residual interaction between the quasiparticles.

We consider the system $n = \Omega_1 = \Omega_2$, in which case $\lambda = 0$. The BCS occupation parameters are in this case

$$U_2^2 = V_1^2 = \frac{1}{2} \left(1 - \frac{1}{x} \right) \quad (5.19)$$

and

$$U_1^2 = V_2^2 = \frac{1}{2} \left(1 + \frac{1}{x} \right), \quad (5.20)$$

while the quasiparticle energy is

$$E = G\Omega. \quad (5.21)$$

The two-level system displays a pairing distortion (gap) of magnitude

$$\begin{aligned} \Delta &= G\langle 0|T|0\rangle = G\Omega(U_1V_1 + U_2V_2) \\ &= G\Omega \left(1 - \frac{1}{x^2} \right)^{1/2}, \end{aligned} \quad (5.22)$$

$|0\rangle$ being the BCS ground state. Note that Δ is a collective deformation receiving contributions from all the pairs of particles, and thus is proportional to Ω . The expression given in equation (5.22) should coincide with the single j -shell expression given in equation (H.4) (for $N = \Omega$, see also Section 3.7) in the case $D = 0$. Note, however, that in this case the total degeneracy of the two degenerate shells is 2Ω , thus leading to $\Delta = G\Omega$.

The fluctuations around this equilibrium distortion are induced by the residual interaction among the quasiparticles H'_p and H''_p (see equations (4.23) and (4.24)) leading to the secular equation (see Appendix J, equation (J.31))

$$W_n^2 [(W_n^2 - 4\Delta^2)A - B] = 0, \quad (5.23)$$

where

$$A = \left(\sum_i \frac{\Omega_i}{2E_i(4E_i^2 - W_n^2)} \right)^2, \quad (5.24)$$

$$B = \left(\sum_i \frac{\Omega_i f_i}{4E_i^2 - W_n^2} \right)^2 \quad (5.25)$$

and

$$f_i = U_i^2 - V_i^2. \quad (5.26)$$

The forward-going and backward-going RPA amplitudes are

$$a_{ni} = \frac{\Lambda_{1n} f_i + \Lambda_{2n}}{2E_i - W_n} \sqrt{\Omega_i}, \quad (5.27)$$

$$b_{ni} = \frac{-\Lambda_{1n} f_i + \Lambda_{2n}}{2E_i + W_n} \sqrt{\Omega_i}, \quad (5.28)$$

while

$$\frac{\Lambda_{2n}}{\Lambda_{1n}} = - \frac{\sum_i \frac{\Omega_i f_i}{4E_i^2 - W_n^2}}{W_n \sum_i \frac{\Omega_i}{2E_i(4E_i^2 - W_n^2)}} \tag{5.29}$$

and

$$\begin{aligned} \Lambda_{1n} = \frac{1}{2} & \left[W_n \left(\sum_i \frac{f_i^2 2E_i \Omega_i}{(4E_i^2 - W_n^2)^2} \right) + \left(\sum_i \frac{f_i(4E_i^2 + W_n^2)\Omega_i}{(4E_i^2 - W_n^2)^2} \right) \frac{\Lambda_{2n}}{\Lambda_{1n}} \right. \\ & \left. + W_n \left(\sum_i \frac{2E_i \Omega_i}{(4E_i^2 - \Omega_i)^2} \right) \left(\frac{\Lambda_{2n}}{\Lambda_{1n}} \right)^2 \right]^{-1/2}. \end{aligned} \tag{5.30}$$

The elements a_{11} and a_{22} in the 2×2 determinant (see equation (J.27)) correspond to the dispersion relations resulting from the linearization conditions $[H_{11} + H'_p, \Gamma_n^\dagger] = W'_n \Gamma_n^\dagger$ and $[H_{11} + H''_p, \Gamma''_n^\dagger] = W''_n \Gamma''_n^\dagger$, respectively, the corresponding collective modes being the pairing vibrations and the Anderson–Goldstone–Nambu (AGN) mode (see Chapter 4). Aside from the root at $W_n = 0$, all roots of (5.23) fulfil the condition $W_n \geq 2\Delta$. In fact, because A and B are positive quantities, the dispersion relation cannot be zero for $W_n < 2\Delta$. If $W_n = 2\Delta$ is a possible root, then the coupling term between the AGN and the pairing vibration, i.e. between the even and odd solutions of the pairing Hamiltonian, must be zero. Thus

$$\sum_i \frac{\Omega_i f_i}{4E_i^2 - W_n^2} \Big|_{W_n=2\Delta} = \sum_i \frac{\Omega_i}{4E_i(\varepsilon_i - \lambda)} = 0, \tag{5.31}$$

which holds true if there is a symmetric distribution of levels around the Fermi surface. This is the case in the model under discussion. Thus

$$W = 2\Delta \tag{5.32}$$

and

$$\Lambda_{2n}/\Lambda_{1n} = 0. \tag{5.33}$$

Utilizing the fact that $f_1 = -f_2 = -\varepsilon/G\Omega$, and equations (5.20), (5.21) and (5.30), we obtain

$$\Lambda_{1n} = \left[\frac{W_n}{2} \left(\sum_i \frac{2E_i \Omega_i f_i^2}{(4E_i^2 - W_n^2)^2} \right) \right]^{-1/2} = \varepsilon \sqrt{\frac{G}{2\Delta}}. \tag{5.34}$$

Thus

$$a_1 = - \frac{\varepsilon^2}{2(G\Omega - \Delta)} \sqrt{\frac{1}{2\Delta G\Omega}} = -b_1. \tag{5.35}$$

From this result and the expression of the two-body transfer operator

$$T = \sqrt{\Omega_j} U_j^2 \left(\sum_n a_{ni} \Gamma_n^\dagger - \sum_n b_{ni} \Gamma_n \right) + \sqrt{\Omega_j} V_j^2 \left(\sum_n a_{ni} \Gamma_n - \sum_n b_{ni} \Gamma_n^\dagger \right) + \Omega_j U_j V_j, \quad (5.36)$$

we obtain

$$\sigma_{\text{gs}} = |\langle \text{gs}(\Omega) | T | \text{gs}(\Omega - 1) \rangle|^2 = \left(\sum_{j=1,2} \Omega_j U_j V_j \right)^2 = \left(1 - \frac{1}{x^2} \right) \Omega^2 \quad (5.37)$$

and

$$\begin{aligned} \sigma_1 &= |\langle n = 1(\Omega) | T | \text{gs}(\Omega - 1) \rangle|^2 = \left[\sum_j \sqrt{\Omega_j} (U_j^2 a_{nj} + V_j^2 b_{nj}) \right]^2 \\ &= \frac{\Omega}{2x^2(1 - 1/x^2)^{1/2}}, \end{aligned} \quad (5.38)$$

for intraband and cross-over two-particle cross-sections, respectively.

All pairs of particles participate in the transition between members of the ground-state rotational band, and the cross-section is proportional to Ω^2 . This transition is very large compared with the transition to the pairing vibration. The corresponding ratio

$$\frac{\sigma_1}{\sigma_{\text{gs}}} = \frac{1}{2x^2} \left(1 + \frac{3}{2x^2} \right) \frac{1}{\Omega} \quad (5.39)$$

is about 10^{-2} for $x = 2$ and $\Omega \approx 10$, which can be considered typical numbers for superfluid systems.

Thus, the pairing vibration, which can be viewed as a coherent transfer of quasiparticles across the Fermi surface, gives rise to a pairing rotational band weakly connected with the ground-state band (see Chapter 4, in particular Fig. 4.2).

5.1.3 Pairing phase transitions

In the case of the quadrupole surface modes of excitation, changes of coupling scheme from the spherical-phonon scheme to the deformed-rotational scheme take place in different regions of the mass table. This change in coupling scheme is usually referred to as a quadrupole phase transition (see, e.g. Bohr and Mottelson (1975)). The pairing order parameter can also be subjected to a ‘macroscopic’ change and the system undergoes a phase transition from the normal (pairing vibrational) to the superconducting (pairing rotational) state. In both cases the polarization effects of particles outside closed shells give rise to a static field

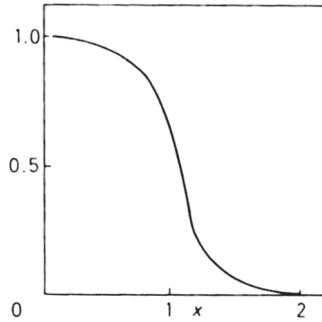


Figure 5.2. Ratio $|\langle n = 1(\Omega) | T | \text{gs}(\Omega - 1) \rangle|^2 / |\langle \text{gs}(\Omega) | T | \text{gs}(\Omega - 1) \rangle|^2$ calculated by utilizing the exact functions of the two-level model ($\Omega = 20$) as a function of x .

which violates, in one case, rotational invariance and, in the other, particle number conservation, leading to a privileged orientation in normal and in gauge space. The associated fluctuations which restore rotational and gauge invariance give rise to quadrupole (see Bohr and Mottelson (1975)) and to pairing rotational bands (Bes and Broglia (1966), Chapter 4). The specific probes to study quadrupole phase transitions are Coulomb excitation and inelastic scattering. In a similar way, (t, p) and (p, t) reactions are the specific probes to study the change in the pairing coupling elements.

The most conspicuous feature associated with a pairing phase transition is the behaviour of the ratio $\sigma_1/\sigma_{\text{gs}}$. Equation (5.16) shows that $\sigma_1/\sigma_{\text{gs}} \approx 1$ for the normal phase while equation (5.39) shows that it tends to zero in the superfluid phase. The exact variation of this ratio as a function of x for the two-level model is displayed in Fig. 5.2. Both the RPA pairing vibration scheme for $x < 1$ (equation (5.16)) and the BCS for $x > 1$ (equation (5.38)) diverge at $x = 1$, while the exact calculation predicts a smooth transition. The approximate results are in good agreement with the exact ones for $x \lesssim 0.5$ and for $x \gtrsim 1.5$.

The variation of the two-particle transition intensities have been studied as a function of the number n of pairs in Broglia *et al.* (1968b). The cross-section σ_{gs} from the ground state of the initial nucleus to the ground state of the final nucleus has a rather smooth variation with n and increases as the strength x of the pairing interaction increases. The cross-section σ_1 associated with the pair addition mode to the first excited state is strongly affected by the pairing phase transition. For $x > 1.4$, the crossing of the closed shell at $n = \Omega$ is smooth while for $x < 1.2$ there is a sudden drop in σ_1 at $n = \Omega$. This is because, in the normal phase, the pairing vibration is a two-phonon state, whereas, in the superfluid case, it is a one-phonon type of excitation, the closed shell being defined as the state containing no phonons. In both cases, the two-body transfer operator can change the number of phonons in one.

There is a pairing phase transition in high spin states of deformed nuclei which is induced by the nuclear rotation. The Coriolis field plays the role of an external magnetic field in a superconductor. This phenomenon will be discussed in Chapter 6 of this book.

5.2 Applications

In what follows we apply the concepts developed above to the case of pairing vibration in closed- and in open-shell nuclei.

5.2.1 Normal systems (Pb isotopes)

The nucleus ^{208}Pb provides the best example of a closed-shell nucleus. There is a neat separation between particles and holes. In fact $D \approx 3 \text{ MeV}$ and $2G\Omega \approx 0.2 \times 5 \approx 1.0 \text{ MeV}$ ($G \approx 21.5/A \text{ MeV}$, $j_1 = p_{1/2}$, $j_2 = g_{9/2}$, see Table 5.1), which results in $x \approx 0.3$.

Systematic (t, p) and (p, t) experiments carried out in this region show a well-developed monopole pairing vibrational band (see Fig. 5.5) which encompasses states with up to three phonons of the same type ($gs(^{202}\text{Pb})$) or of different type

Table 5.1. *Forward-going and backward-going amplitude (5.51) describing the motion of two particles (^{210}Pb) and two holes (^{206}Pb) around ^{208}Pb . A coupling constant $G = 21.4/A \text{ MeV}$ was utilized to reproduce the extra binding energy (5.46) of ^{210}Pb , while the corresponding quantity (5.45) for ^{206}Pb was reproduced for $G = 21.7/A \text{ MeV}$ (see also Fig. 8.17).*

Single-particle states		^{206}Pb		^{210}Pb	
0	$h_{9/2}$	$r_1(\gamma)$	0.11	$a_1(\gamma)$	0.09
1	$f_{7/2}$		0.14		0.10
0	$i_{13/2}$		0.27		0.16
2	$p_{3/2}$		0.24		0.10
1	$f_{5/2}$		0.41		0.14
2	$p_{1/2}$		0.84		-0.10
1	$g_{9/2}$	$r_1(\omega)$	0.13	$a_1(\omega)$	0.82
0	$h_{11/2}$		0.11		0.44
0	$j_{15/2}$		0.11		0.35
2	$d_{5/2}$		0.06		0.20
3	$s_{1/2}$		0.03		0.09
1	$g_{7/2}$		0.06		0.17
2	$d_{3/2}$		0.04		0.11

(excited state in ^{206}Pb). The identification of 0^+ states excited in either (t, p) or (p, t) reactions is rather simple due to the well-developed diffraction pattern of the associated angular distribution (see Broglia *et al.* (1973)). Two quantum numbers are needed to classify the different states of this two-dimensional harmonic oscillator. We utilize (n_r, n_a) which indicate the number of pair removal and pair addition modes in each state.

The energy of the (1, 1) state in ^{208}Pb predicted by the pairing vibrational model is

$$\begin{aligned} W(1, 1) &= (B(208) - B(206)) - (B(210) - B(208)) \\ &= (14.110 - 9.123) \text{ MeV} = 4.987 \text{ MeV}, \end{aligned} \quad (5.40)$$

where $B(A)$ is the binding energy of the Pb isotope with mass A .

For pedagogical purposes we require the pair addition and pair subtraction modes to have the same energy. Thus

$$W = W(0, 1) = W(1, 0) = 2.494 \text{ MeV}. \quad (5.41)$$

The excitation energy of any state of the model can be then written as

$$W(n_r, n_a) = (n_a + n_r)2.494 \text{ MeV}. \quad (5.42)$$

The experimental magnitude to be compared is

$$E(N) = (B(^{208}\text{Pb}) - B(N)) + 5.808(N - 126) \text{ MeV}. \quad (5.43)$$

The linear term ensures $E(124) = E(128)$, which corresponds to the condition (5.41). The different transitions associated with these states are given in terms of the basic cross-section

$$a = \sigma(\text{gs}(^{208}\text{Pb}) \rightarrow \text{gs}(^{210}\text{Pb})) \quad \text{and} \quad r = \sigma(\text{gs}(^{208}\text{Pb}) \rightarrow \text{gs}(^{206}\text{Pb})). \quad (5.44)$$

The experimental data associated with (t, p)–(p, t)-reactions on the Pb isotopes around ^{208}Pb are displayed, in term of these elements, in Fig. 5.5.

A microscopic description of the pair addition and pair subtraction modes is obtained by diagonalizing the pairing Hamiltonian in the RPA. The particles and holes are allowed to move in the six levels below and the seven levels above the Fermi surface which are experimentally known (see Table 5.1). The discussion here follows Broglia and Riedel (1967a) and Broglia (1985c). The strength of the coupling constant is determined by fitting the extra binding energy $E(124) = E(128)$, which corresponds to the condition (5.41).

The pairing energies of the two holes and two particles are

$$\begin{aligned} \Delta(206) &= 2[B(208) - B(207)] - [B(208) - B(206)] \\ &= 14.750 \text{ MeV} - 14.110 \text{ MeV} = 640 \text{ keV} \end{aligned} \quad (5.45)$$

and

$$\begin{aligned}\Delta(210) &= 2[B(210) - B(208)] - [B(209) - B(208)] \\ &= 9123 \text{ MeV} - 7886 \text{ MeV} = 1237 \text{ keV}.\end{aligned}\quad (5.46)$$

The pair addition and pair removal creation operators can be written as

$$\Gamma_n^\dagger(\beta = 2) = \sum_{\omega} a_n(\omega)\Gamma^\dagger(\omega) + \sum_{\gamma} a_n(\gamma)\Gamma(\gamma) \quad (5.47)$$

and

$$\Gamma_n^\dagger(\beta = -2) = \sum_{\gamma} r_n(\gamma)\Gamma^\dagger(\gamma) + \sum_{\omega} r_n(\omega)\Gamma(\omega), \quad (5.48)$$

where

$$\begin{aligned}\Gamma^\dagger(\omega) &= a^\dagger(\omega)a^\dagger(\bar{\omega}), \\ \Gamma^\dagger(\gamma) &= a(\bar{\gamma})a(\gamma),\end{aligned}\quad (5.49)$$

and n labels the states according to their energy. The indices ω and γ are the shell model quantum numbers of single-particle orbits above and below the Fermi surface, while $\beta = 2$ refers to pair addition and $\beta = -2$ to pair removal modes, β being the transfer quantum number. The RPA equations are the same as those given in equations (5.10)–(5.14) but now for a general distribution of single-particle levels. The energy W_n obtained by linearizing the pairing Hamiltonian is the n th root of the dispersion relation

$$\frac{1}{G(\pm 2)} = \sum_{\omega} \frac{1}{2\varepsilon(\omega) \mp W_n(\beta = \pm 2)} + \sum_{\gamma} \frac{1}{2\varepsilon(\gamma) \pm W_n(\beta = \pm 2)}. \quad (5.50)$$

The coefficients a_n and r_n are equal to (see Table 5.1, as well as Fig. 8.17)

$$\begin{aligned}a_n(\omega) &= \frac{\Lambda_n(\beta = 2)}{2\varepsilon(\omega) - W_n(\beta = 2)}, & a_n(\gamma) &= -\frac{\Lambda_n(\beta = 2)}{2\varepsilon(\gamma) - W_n(\beta = 2)}, \\ r_n(\omega) &= -\frac{\Lambda_n(\beta = -2)}{2\varepsilon(\omega) - W_n(\beta = -2)}, & r_n(\gamma) &= \frac{\Lambda_n(\beta = -2)}{2\varepsilon(\gamma) - W_n(\beta = -2)},\end{aligned}\quad (5.51)$$

where

$$\begin{aligned}&< 0|\Gamma(\beta = \pm 2)H_p a^\dagger(j)a^\dagger(\bar{j})|0 > = \Lambda_n(\beta = \pm 2) \\ &= \left[\pm \sum_{\omega} [2\varepsilon(\omega) \mp W_n(\beta = \pm 2)]^{-2} \right. \\ &\quad \left. \mp \sum_{\gamma} [2\varepsilon(\gamma) \mp W_n(\beta = \pm 2)]^{-2} \right]^{-1/2},\end{aligned}\quad (5.52)$$

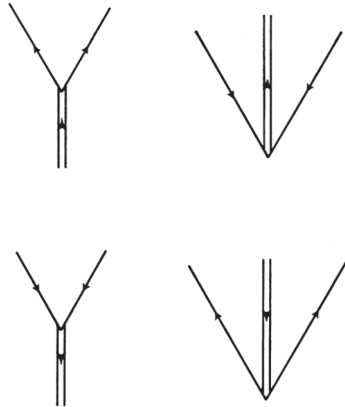


Figure 5.3. Graphical representation of the forward-going and backward-going amplitudes (5.51) of the pairing modes. The vertex strength is equal to $\Lambda_n(\beta = \pm 2)$ (see equation (5.52)). The pairing boson is represented by a double arrowed line, while a single arrowed line represents a fermion.

is the normalization constant of the phonon wavefunction as well as the strength with which a pair of particles in time-reversed states couples to the pairing mode.

Note that the amplitudes (5.51) are obtained by dividing the normalization constants $\Lambda_n(\beta = 2)$ and $\Lambda_n(\beta = -2)$ by the corresponding energy denominators (see Fig. 5.3). This is a common feature of separable forces. The central role played by $\Lambda_n(\beta)$ in the study of the interplay between the different modes of excitation will become apparent in the following sections. The cross-section associated with the transfer of two particles starting from the $N_0 - 2$ ground-state system and leading to the closed-shell (N_0) ground state is

$$r \equiv \sigma^{(0s)}((1, 0) \rightarrow (0, 0)) \propto \Lambda_1^2(\beta = -2). \quad (5.53)$$

For the cross-section leading to the pair addition mode one obtains

$$a \equiv \sigma^{(0s)}((0, 0) \rightarrow (0, 1)) \propto \Lambda_1^2(\beta = 2). \quad (5.54)$$

The values of the pairing strengths obtained by fitting the energy of the 206 and 210 ground states are $G(2) = 0.10$ MeV and $G(-2) = 0.14$ MeV. The resulting absolute cross-sections are reproduced within a factor of 2. Details of the calculations of the two-particle transfer cross-section are given in Broglia and Riedel (1967a), Broglia *et al.* (1973) and Broglia (1985c). By utilizing the microscopic results it is possible to give a measure of the collectivity of the pair addition and pair removal modes by expressing the corresponding cross-sections in terms of absolute two-particle units. Typical enhancements

$$\varepsilon = \sigma_{\text{exp}}/\sigma_{2p}, \quad (5.55)$$

of order 12 are obtained, where σ_{2p} is the average value of the two-particle cross-section to pure two-particle states (see Broglia *et al.* (1971d)). This number can be compared with the value of $10 B_{sp}$ which is typical of the B(E2) transition rate connecting the lowest 2^+ with the ground state of spherical nuclei.

Note that the contributions of all the different two-particle and two-hole components of the microscopic wavefunction to the corresponding transfer amplitudes associated with the excitation of the $n = 1$ mode are constructively coherent.

5.2.2 Superfluid systems (*Sn isotopes*)

The Sn isotopes are probably the best example of superfluid spherical nuclei, with a large number of particles outside the closed shell and a large value of the pairing parameter Δ (≈ 1.4 MeV). (t, p) and (p, t) data is shown in Fig. 5.4 (see also Fig. 4.2). The ground-state transition dominates the spectrum, the interband-to-intraband ratio never becoming larger than 0.18. The behaviour of the (t, p) and (p, t) intensities is rather asymmetric, indicating a competition between pairing and shell effects, as shown below. We discuss first the reaction $^{118}\text{Sn}(t, p)^{120}\text{Sn}$.

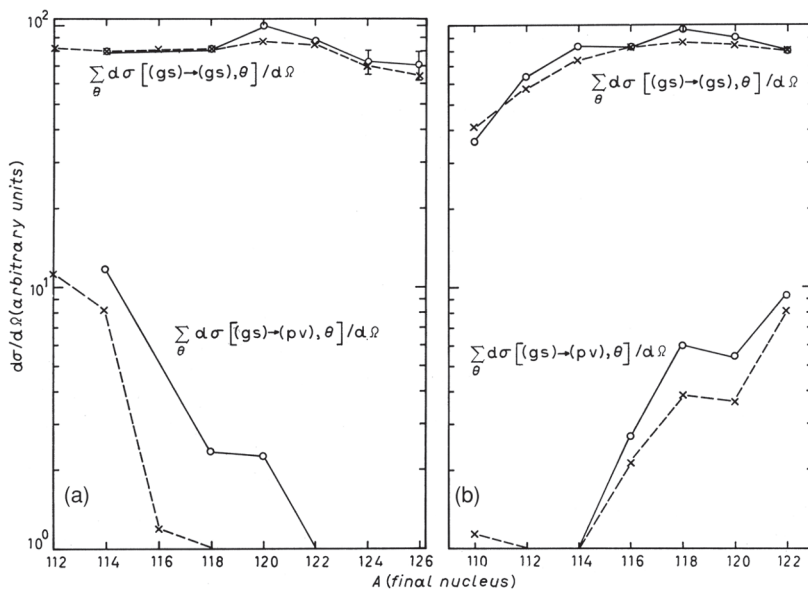


Figure 5.4. Experimental (Bjerregaard *et al.* (1968, 1969), Flynn *et al.* (1970) Fleming *et al.* (1970)) (solid line and open circles) and theoretical (dashed line and crosses) cross-sections corresponding to the $J^\pi = 0^+$ states below 3 MeV excited in the reactions (a) $A+2\text{Sn}(t, p)$ and (b) $A-2\text{Sn}(t, p)$. When more than one excited state was observed, the numbers reported are the centroid energy and the summed cross-section. The normalization between theory and experiment was done in both cases to the $^{118}\text{Sn}(p, t) \rightarrow ^{120}\text{Sn}(p, t)$ reactions.

Table 5.2. Wavefunctions (see equations (5.27) and (5.28)) and energies associated with the lowest $J^\pi = 0^+$ states of ^{118}Sn . The valence particles were allowed to move in the five single-particle states displayed. The corresponding BCS occupation parameter U is also given for each single-particle state.

		$2d_{5/2}$	$1g_{7/2}$	$3s_{1/2}$	$2h_{11/2}$	$2d_{3/2}$
U		0.2449	0.3489	0.4438	0.7861	0.8494
0_1^+	a	-0.0143	-0.0278	-0.0212	0.4340	0.9003
$W = 2.61$ MeV	b	0.0122	0.0155	0.0075	-0.0034	-0.0005
0_2^+	a	-0.1903	-0.4773	-0.7384	-0.4128	0.1638
$W = 2.73$ MeV	b	0.0163	0.0160	0.0039	0.0629	-0.0450
0_3^+	a	-0.1768	-0.7429	0.6243	-0.1605	0.0666
$W = 3.24$ MeV	b	0.0050	0.0029	-0.0013	0.0458	-0.0313

The Hamiltonian $H = H_{11} + H_p' + H_p''$ (see Section 4.2.1 and Appendix J) was diagonalized in the RPA. A coupling constant $G = 23/A$ MeV was utilized, determined by fitting the ^{118}Sn pairing gap ($\Delta_n = 1.39$ MeV). This procedure yields the occupation parameters, energies and wavefunctions given in Table 5.2 (see also Broglia *et al.* (1968a)).

Making use of these wavefunctions the following enhancement factors (see equation (5.55)) were obtained,

$$\varepsilon = 220 \text{ (gs)}, \quad \varepsilon = 4 \text{ (} 0_1^+ \text{)}, \quad \varepsilon = 4 \text{ (} 0_2^+ \text{)}. \quad (5.56)$$

The square root of the value associated with the ground state gives a measure of the number of twofold degenerate levels contributing to the static pairing distortion Δ . This number is ≈ 15 (see (3.68)). Thus, all the levels considered in solving the BCS equation contribute to the ground-state transition (in fact $\sum_j (j + 1/2) = 18$). The enhancement factor $\varepsilon(\text{gs}) = 220$ associated with an interband transition should be compared with the enhancement factors obtained for the $E2$ decay of the 2^+ member of the ground-state rotational band in quadrupole deformed nuclei. Typical numbers are $200 B_{\text{sp}}$ implying that about $\sqrt{200} \approx 14$ twofold degenerate levels contribute to the quadrupole static deformation Q_0 .

The systematic comparison between the intensities predicted by the pairing vibrational model and the experimental data is carried out in Fig. 5.4. A rather considerable change of the order parameter $\Delta / \langle \delta \varepsilon \rangle$ takes place through Sn isotopes. The quantity $\langle \delta \varepsilon \rangle$ is the average distance between the levels around the Fermi surface. Thus $\Delta / \langle \delta \varepsilon \rangle$ plays a similar role to that played by x in the case of the two-level model (see Section 5.1, equation (5.9)). It may be approximated by the number $n_\Delta(A)$ of double degenerate single-particle levels

in the interval $\Delta(A)$ around $\lambda(A)$. We obtain (see also equation (3.68))

$$n_{\Delta}(^{112}\text{Sn}) = 8, \quad n_{\Delta}(^{116}\text{Sn}) = 3 \quad (5.57)$$

and

$$n_{\Delta}(^{120}\text{Sn}) = 8. \quad (5.58)$$

These changes in $\Delta / \langle \delta \varepsilon \rangle$ give rise to a partial distinction between particles and holes and, consequently, to two collective transitions similar to the case of normal systems, in particular for the case of ^{114}Sn .

5.3 Multipole pairing vibrations

In the previous sections we have concentrated our attention in the monopole pairing modes. Thus, we have restricted the distortions and vibrations of the Fermi surface to be isotropic. The condensation in p -wave observed in the case of ^3He gives an example, at the macroscopic scale, of non-isotropic distortions of the Fermi surface, produced by a pairing interaction acting in an $l = 1$ state of relative motion (see Chapter 1). In fact, the three superfluid phases corresponding to $\uparrow\uparrow$, $\downarrow\downarrow$ and $\uparrow\downarrow$ ($m = \pm 1, 0$) have been observed (see e.g. Vollhardt and Wölfle (1990)). Experimental evidence indicates that high- T_c superconductors (cuprates) display a mixture of s - and d -pairing (see, e.g. Tinkham (1996) Section 9.6). In nuclei the only component of the short-range part of the residual interaction which gives rise to a condensate is the monopole pairing force. It is, however, expected that multipole vibrations, which change the number of particles by two, can play an important role in the dynamics of the nuclear spectrum (see also Section 8.4).

5.3.1 Normal systems (*Pb isotopes*)

There is specific evidence for the existence of multipole pairing vibrations provided by the strong $L = 2, 4$ and 6 cross-sections associated with (t, p) and (p, t) transitions in the Pb isotopes (Bjerregaard *et al.* (1966b), Igo *et al.* (1971), Landford and McGrory (1973)). A microscopic description of these modes can be obtained as in the case of the monopole pairing vibration, in the framework of the random-phase approximation, allowing the particles to correlate through the schematic interaction (Bes and Broglia (1971))

$$H(2\lambda) = -\frac{\pi G_{\lambda}}{2\lambda + 1} \sum_{\mu} P_{\lambda\mu}^{\dagger} P_{\lambda\mu}, \quad (5.59)$$

where

$$P_{\lambda\mu}^{\dagger} = \sum_{j_1 j_2} \langle j_1 || Y_{\lambda} || j_2 \rangle [a_{j_1}^{\dagger} a_{j_2}^{\dagger}]_{\mu}^{\lambda}. \quad (5.60)$$

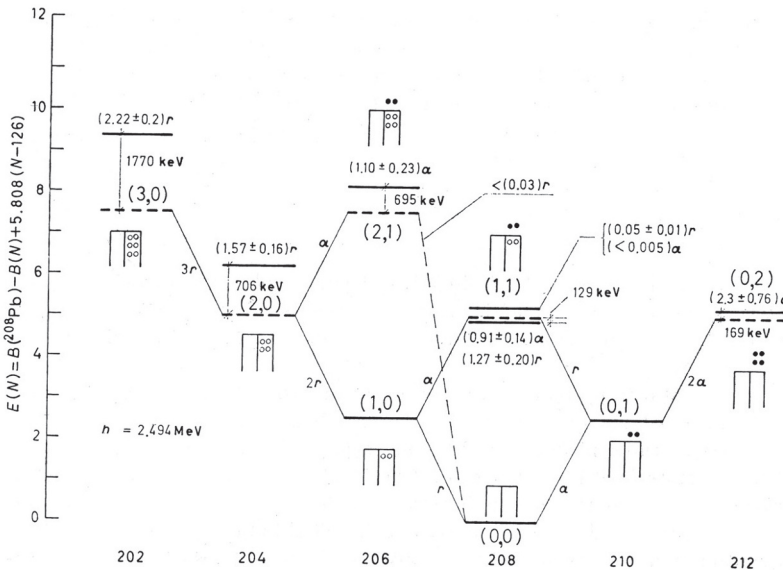


Figure 5.5. The many-phonon pairing spectrum around ^{208}Pb . The energies predicted by the pairing vibrational model are displayed as dashed horizontal lines. The harmonic quantum numbers (n_r, n_a) are indicated for each level. A schematic representation of the many-particle many-hole structure of the state is also given. The transitions predicted by the model are indicated in units of r and a (see equation (5.44)). The corresponding experimental numbers are also given together with their errors, above each level. The dashed line between the states $(0, 0)$ and $(2, 1)$ indicates that the $^{208}\text{Pb}(p, t)^{206}\text{Pb}$ reaction to the three-phonon state in ^{208}Pb was carried out and an upper limit of $0.03r$ for the corresponding cross-section was determined (see Flynn *et al.* (1972) Broglia *et al.* (1973), also Landford and McGrory (1973)).

The coupling constant G_λ can be determined through dispersion relations similar to that shown in equation (5.50), by fitting the binding energy of the two-particle and two-hole system, respectively. The resulting values corresponding to the multiplicities $\lambda = 0, 2, 4$ and 6 and to both ^{206}Pb (pair-removal modes) and ^{210}Pb (pair-addition modes) are very similar to each other and equal to (see Broglia *et al.* (1974b))

$$G_\lambda \approx 27/A \text{ MeV}. \tag{5.61}$$

Using the corresponding wavefunctions one obtains the (t, p) and (p, t) cross-sections displayed in Table 5.3.

The quadrupole transition probability between the lowest 2^+ and the ground state of ^{210}Pb is given in the present model by

$$B(E2; 0 \rightarrow 2^+) = (e_{\text{eff}})^2 \left[2 \sum_{j_1 j_2} a(j_1 j_2; 2^+) a(j_1^2; \text{gs}) \frac{\langle j_2 || r^2 Y_2 || j_1 \rangle}{\sqrt{2j_1 + 1}} \right]^2. \tag{5.62}$$

Table 5.3. Ratio of experimental (Landford and McGrory (1973), Bjerregaard et al. (1966a), Igo et al. (1971)) and theoretical (Broglia et al. (1974b)) cross-sections associated with the reactions $^{208}\text{Pb}(p, t)^{206}\text{Pb}$ leading to the lowest states of each spin and parity.

J^π	$^{208}\text{Pb}(p, t)^{206}\text{Pb}(J^\pi)$		$^{208}\text{Pb}(t, p)^{210}\text{Pb}(J^\pi)$	
	E (MeV)	$\frac{[d\sigma(J^\pi)/d\Omega]_{\text{exp}}}{[d\sigma(J^\pi)/d\Omega]_{\text{th}}}$	E (MeV)	$\frac{[d\sigma(J^\pi)/d\Omega]_{\text{exp}}}{[d\sigma(J^\pi)/d\Omega]_{\text{th}}}$
0^+	0.000	0.94	0.000	1.47
2^+	0.803	0.75	0.795	0.78
4^+	1.684	0.88	1.094	1.21
6^+	3.253	0.49	1.193	0.77

Using the calculated amplitudes and the experimental data ($B(E2)_{206} = 7B_{\text{sp}} = 0.5B(E2)_{210}$), one obtains for the effective charges (see Bohr and Mottelson (1975) and references therein)

$$e_{\text{eff}}(^{206}\text{Pb}) = 0.98, \quad e_{\text{eff}}(^{210}\text{Pb}) = 1.03. \quad (5.63)$$

These values are consistent with the effective charges obtained from transitions among single-particle states in ^{207}Pb and ^{209}Pb (see Bohr and Mottelson (1975) and references therein). This result provides further support for the description of the 2_1^+ of ^{210}Pb as a pairing vibration of ^{208}Pb .

The existence of a $\mu = 0$ quadrupole pairing force of strength approximately equal to (5.61) has been shown (Ragnarsson and Broglia (1976)) to play a basic role in the 0^+ spectrum of the actinide nuclei (see next section). As discussed in Hamamoto (1977), the $\mu = 1$ component of the quadrupole pairing force plays an important role in determining the value of the moment of inertia of deformed nuclei (see also Migdal (1959) and Belyaev (1961)).

5.3.2 Superfluid systems (heavy deformed nuclei)

In normal spherical nuclei the Hamiltonian (5.59) generates the $\alpha \pm 2$ modes, but has no systematic effect on the particle-hole states, i.e. states with transfer quantum number $\alpha = 0$. The part of the nuclear interaction which generates isoscalar surface vibrations can be written schematically as (see also Section 3.4)

$$H(0\lambda) = -\frac{\kappa_\lambda}{2} \sum_{\mu} Q_{\lambda,\mu}^\dagger Q_{\lambda,\mu}, \quad (5.64)$$

where

$$Q_{\lambda\mu} = -\frac{1}{\sqrt{2\lambda+1}} \sum_{a_1 a_2} \langle a_1 || r^\lambda Y_\lambda || a_2 \rangle [a_1^\dagger a_2]_\mu^\lambda. \quad (5.65)$$

In superfluid nuclei, because the distinction between particles and holes is lost, the two-quasiparticle states $(\lambda, \pi = (-1)^\lambda)$ are correlated by both the multipole pairing and the particle–hole interaction. Note that while the correlations generated by (5.59) specifically enhance two-nucleon transfer reactions, (5.65) enhances inelastic scattering and Coulomb excitation processes (see Broglia *et al.* (1971d), (1973)). Consequently, the presence of both particle–hole and multipole pairing interaction lead to ground-state correlations (zero point fluctuations) which, being opposite to each other (blocking effects), stabilize low-lying vibrations displaying both enhanced $B(E\lambda)$ as well as (t, p) and (p, t) cross-sections. The consequences of the interplay between multipole particle–hole and pairing (particle–particle) correlations in the nuclear spectrum is still an open question (see e.g. Volya *et al.* (2001, 2002), Zelevinsky and Volya (2004)).

Because of the conservation of angular momentum, the BCS pairing gap, which can be related to the odd–even mass difference, is determined by the monopole pairing interaction. This is also true, as discussed above, for the fluctuations of the gap giving rise to two-quasiparticle 0^+ pairing vibrational states.

For deformed nuclei this restriction is no longer valid. The pairing gap now receives contributions from different pairing multipoles, i.e.

$$\Delta_i = \Delta_0 + \sum_{\lambda>0} \Delta_\lambda Q_i^{(\lambda)}, \quad (5.66)$$

where

$$Q_i^{(\lambda)} = \langle i || Y_\lambda || i \rangle, \quad (5.67)$$

$$\Delta_0 = G_0 \sum_i U_i V_i \quad (5.68)$$

is the standard (monopole) pairing gap and

$$\Delta_\lambda = \sqrt{\frac{\pi}{2\lambda+1}} G_\lambda \sum_i \langle i || Y_\lambda || i \rangle U_i V_i \quad (5.69)$$

measures the multipole distortion (departure from anisotropy) of the Fermi surface (see Broglia *et al.* (1969a)). The index i labels Nilsson single-particle levels. Specialized to the case of $\lambda = 2$, the pairing matrix elements are equal to

$$\langle i\tilde{i} | (H(2, 0) + H(2, 2)) | j\tilde{j} \rangle = -G_0 - G_2 Q_i Q_j, \quad (5.70)$$

where we have used $Q_i = Q_i^{(2)}$. The violation of both angular momentum and particle number conservation brings a new dimension to the role that multipole pairing correlations play in nuclear structure (Bes *et al.* (1972)).

In particular, the gap (5.66) can become very small for certain levels as well as the matrix element (5.70). This phenomenon is analogous to the phenomenon of gapless superconductivity in solid-state physics. There, an impurity traps a magnetic field which is larger than the critical magnetic field H_c , thus giving rise to some quasiparticles for which $\Delta_i \approx 0$. In nuclei, it is the shell structure which acts as impurity, displaying particular signs of the quadrupole moment for particular values of the angular momentum (see Sections 6.2.1 and 6.2.2).

One can distinguish two different types of pairing matrix elements: (i) those that are related with the scattering of particles between pairs of single particles having the same sign of the quadrupole moment, i.e.

$$G_{oo} = \langle i_o \bar{i}_o | H(20) + H(22) | i'_o \bar{i}'_o \rangle = -G_o - G_2 Q_{i_o} Q_{i'_o}, \quad (5.71)$$

$$G_{op} = \langle i_p \bar{i}_p | H(20) + H(22) | i'_p \bar{i}'_p \rangle = -G_o - G_2 Q_{i_p} Q_{i'_p}, \quad (5.72)$$

and (ii) those between pairs of orbitals with opposite sign of the quadrupole moment, i.e.

$$G_{pp} = \langle i_p \bar{i}_p | H(20) + H(22) | i'_p \bar{i}'_p \rangle = -G_o + G_2 |Q_{i_p} Q_{i'_p}|. \quad (5.73)$$

The label o denotes oblate orbitals which have a negative sign of Q , while p stands for prolate orbitals corresponding to a positive sign.

In general,

$$|G_{oo}| \approx |G_{pp}| \gg |G_{op}|. \quad (5.74)$$

In this case we can distinguish, as in the case of closed-shell system, between two groups of single-particle levels which are uncoupled from each other. In the closed-shell system $\langle i \bar{i} | H(20) | i' \bar{i}' \rangle$ has similar values for the scattering of any pair of particles. However, if $i > i_F$, $i' < i'_F$, the scattering amplitude $G_0/\Delta\varepsilon$ becomes very small, $\Delta\varepsilon$ being twice the single energy gap (for Pb, $\Delta\varepsilon \approx 7$ MeV and $G \approx 0.1$ MeV). There is thus a static decoupling between the single-particle levels.

In the case of deformed nuclei, on the other hand, the single-particle levels are closely spaced and $\Delta\varepsilon$ is of order of G (e.g. the average spacing of the single-particle levels of ^{234}U around the Fermi energy shown in Fig. 5.6 is 360 keV). However, because of the inequality (5.74), the scattering amplitude between oblate and prolate single-particle orbitals can become very small. In this case there is a dynamical decoupling between the single-particle levels due to the correlations among the particles.

Let us consider the effect of the monopole plus quadrupole pairing force acting on a system of particles moving in the single-particle levels displayed in Fig. 5.6. Around the Fermi surface there is a predominance of prolate levels, while ≈ 0.7 MeV below the Fermi surface there is a group of oblate single-particle levels.

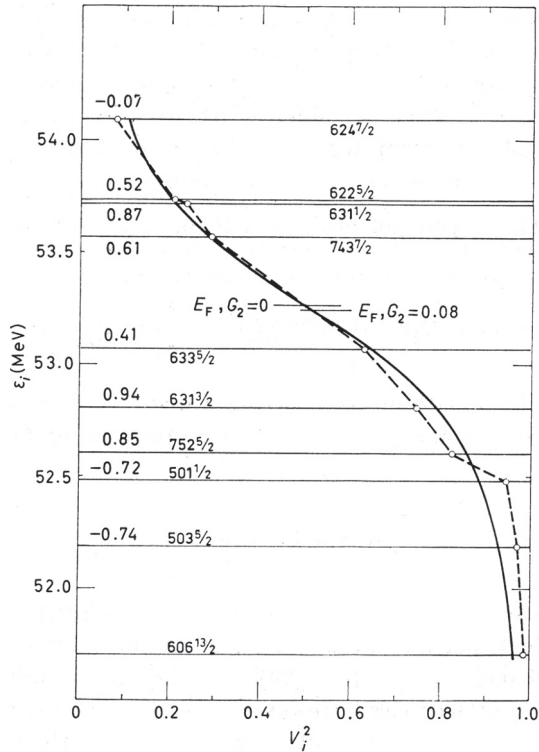


Figure 5.6. The occupation probability V_i^2 for levels around the Fermi surface E_F of ^{234}U for $G_2 = 0.08$ MeV (dashed line). For each level the asymptotic quantum numbers are given as well as the value of the single-particle quadrupole moment in fm^2 .

When the residual monopole and quadrupole pairing interactions are switched on, one can construct essentially two ground states. The ground state of nucleus A , based on the levels around the Fermi surface, and the ground state of the $A - 2$ system (pair-removal mode), based on the states with negative value of the quadrupole moment. Thus, this latter state has a similar relation to its ground state as the $N_0 - 2$ system has to the closed N_0 system ground state. Note that all the different terms which contribute to the two-nucleon transfer amplitude of the excited state can produce constructive coherence and still be orthogonal to the ground state, because the two states have components appreciably different from zero on different single-particle orbitals and thus are orthogonal *ab initio*.

Although the deformed nucleus ^{234}U is superfluid, the quadrupole pairing correlations allow for the existence of real particles ($V_i \approx 1$), almost uncoupled from the superfluid ground state and moving rather close to the Fermi surface. Because of the non-conservation of the number of particles, the states based on the oblate orbitals become an excited state of the A -system, namely an isomeric

pairing state with a rather different average value of the gap parameter than the ground state.

The existence of a pairing isomer in a pairing deformed nucleus is evidenced by the unusually large two-nucleon transfer cross-section to excited 0^+ states, in a similar way that a shape isomer in a quadrupole deformed nucleus displays a very retarded electromagnetic-transition probability. Giving the same weight to the different configurations, we get, for the ground-state (t, p) and (p, t) cross-sections,

$$\sigma(\text{gs} \rightarrow \text{gs}) = \left(\sum_i U_i V_i \right)^2 = (\Delta/G)^2. \quad (5.75)$$

The corresponding cross-sections to an excited 0^+ state are given by

$$\sigma^{(\text{p,t})}(\text{gs} \rightarrow 0^+) \approx \left(2 \sum_i a_i V_i^2 \right)^2 \quad (5.76)$$

and

$$\sigma^{(\text{t,p})}(\text{gs} \rightarrow 0^+) \approx \left(2 \sum_i a_i U_i^2 \right)^2, \quad (5.77)$$

where a_i denotes the two-quasiparticle component (forward-going amplitude) of the single-particle state i .

In the actinide region a typical value for (5.75) is 100, while (5.76) and (5.77) depend strongly on the amplitude a_i . If the first excited state is below the smallest two-quasiparticle energy $2E_i$ and is mainly generated by vibrations of the monopole pairing gap, all the a_i below the Fermi surface have one sign and all those above the opposite sign. This sign change is necessary for the excited state to be orthogonal to the ground state. If $G_2 = 0$, the low-lying excited states will mainly be built out of the states close to the Fermi surface (with $U_i \approx V_i \approx 0.5$), which means that (5.77) and (5.78) will be about equal and of the order of unity because of cancellations from states below and above the Fermi surface.

The pairing isomer ($G_2 \approx 0.1$), on the other hand, is mainly built out of the oblate levels below the Fermi surface and is, from the start, orthogonal to the ground state which has very small components on these single-particle levels. For these oblate levels, $V_i^2 \approx 1(\varepsilon_i < \varepsilon_F)$ and the different contributions to (5.77) add with the same sign resulting in a large (p, t) cross-section.

In a schematic model where the 0^+ state has equal amplitudes on configurations built out of the five oblate orbitals, we find

$$\sigma^{(\text{p,t})}(\text{gs} \rightarrow 0^+) \approx \left(2 \sum_{i=1}^5 \sqrt{\frac{1}{5}} \right)^2 = 20, \quad (5.78)$$

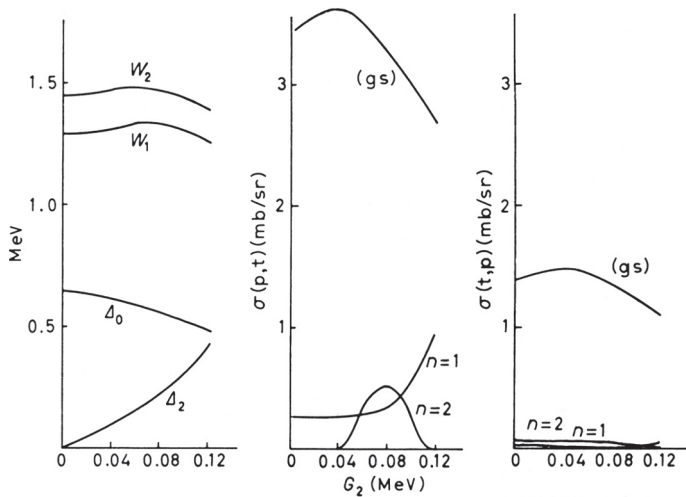


Figure 5.7. Dependence of the different parameters associated with the monopole and quadrupole pairing degree of freedom as a function of G_2 , and for the nucleus ^{234}U . The labels $n = 1$ and $n = 2$ indicate the first and the second 0^+ excited state, respectively.

while the (t, p) cross-section is essentially zero ($U_i \approx 0$) ($\varepsilon_i < \varepsilon_F$). Moreover, as the oblate single-particle levels have a small average value of Δ , the quasiparticle energies $E_i = \sqrt{(\varepsilon_i - \lambda)^2 + \Delta^2}$ will be relatively small implying that the pairing isomer will be found at a low excitation energy.

In Fig. 5.7 we display the change of the different physical magnitudes (W , $\sigma(t, p)$, $\sigma(p, t)$, Δ_0 and Δ_2) as a function of G_2 for fixed values of G_0 and of K_2 . According to the discussion connected with the results displayed in Table 5.3, one should choose $G_2 = G_0$. For this value of G_2 we display in Table 5.4 the results of the model discussed above for nuclei in the actinide region, in comparison with the experimental data (see also Casten *et al.* (1972)).

Before concluding this section it is interesting to mention the results of a recent $^{160}\text{Gd}(p, t)^{158}\text{Gd}$ experiment by Leshner *et al.* (2002), in which 13 excited 0^+ states with energy below 3.2 MeV have been observed. Calculations making use of both particle-hole and pairing multipole interactions seem to be able to explain the presence of so many low-lying 0^+ states (N. Lo Giudice, A. V. Sushkov and N. Yu. Shirikova, *Key Topics in Nuclear Structure*, Paestum 23–27 May 2004, abstracts, p. 76). While none of these states is found to lead to collective electromagnetic transition probabilities, some of them are found to display collectivity in the pairing channel. Note that Zamfir *et al.* (2002) are able to account for essentially all of the 0^+ states observed within a basis

Table 5.4. The experimental (Maher *et al.* (1970) excitation energies, relative (p, t) cross-sections and $X = \rho^2 e^2 R_0^4 / B(E2; 2 \rightarrow 0)$ values associated with the low-lying 0^+ states are compared with the theoretical calculations (Ragnarsson and Broglia (1976)) for the actinide region.

Nucleus	Excitation energy (keV)		$\frac{\sigma(\text{excited } 0^+)}{\sigma(\text{g.s. } 0^+)}$		X		
	Experimental	Theoretical	Experimental	Theoretical	Experimental	Theoretical	
^{228}Th	830		18		(0.83)		
		930		13.4		0.33	
^{230}Th	636		18		0.22 ± 0.10		
	1590		3				
		1040 1270		16.8 4.4			0.35 0.39
^{232}U	695		13		0.17 ± 0.04		
		930		8.5			0.37
^{234}U	812		13		0.50 ± 0.08		
		1020 1250		16.5 2.0			0.41 0.46
^{236}U	920		13		0.05 ± 0.01		
		950		11.7			0.39
		1220		2.1			0.35
		1760		1.6			0.97
^{240}Pu	862		15		0.05 ± 0.01		
	1091		10				
		1070 1260		6.0 1.5			0.41 0.40
		1450		2.6			
^{242}Pu	956		24		0.05 ± 0.01		
		1100		9.0			0.39
		1210		13.7			0.24
		1610		5.9			
^{246}Cm	1176		11		0.05 ± 0.01		
		1180		4.8			0.42
		1300		5.2			0.24
		1610		11.1			

which include s, d and f bosons. This result seem sensible in keeping with the fact that if one adds a g boson to the basis, the calculations would be essentially equivalent to those of Lo Giudice *et al.* mentioned above; see Broglia (1981).